J. Fluid Mech. (1971), *vol.* 48, *part* 4, *pp.* 625–646
Printed in Great Britain

Stability of vertical natural convection boundary layers: some numerical solutions

By C. A. HIEBER† AND B. GEBHART
Department of Thermal Engineering, Cornell University

(Received 9 March 1970 and in revised form 19 January 1971)

Linear stability theory is applied to the natural convection boundary layer arising from a vertical plate dissipating a uniform heat flux. By using a numerical procedure which is much simpler than those previously employed on this problem, computer solutions are obtained for a much larger range of the Grashof number (G). For a Prandtl number (σ) of 0·733, it is found that, as $G \to \infty$: the effect of temperature coupling vanishes more rapidly than that of viscosity; the upper branch of the neutral curve is oscillatory but does approach a finite non-zero inviscid asymptote. For moderate and large values of σ, a loop appears in the neutral stability curve as a result of the merging of two unstable modes. As $\sigma \to \infty$, the mode associated with the uncoupled (i.e. Orr–Sommerfeld) problem rapidly becomes less unstable than that arising from the temperature coupling, with the stability characteristics being independent of the thermal capacity of the plate. For small values of σ, only one unstable mode is found to exist with the coupling effect being negligible in the case of large thermal capacity plates but markedly destabilizing when the thermal capacity is small.

By obtaining numerical results out to $G \approx 10^{10}$ for the cases $\sigma = 0{\cdot}733$ and 6·7, it becomes possible to attempt to directly relate the theory to the actual observance of turbulent transition. Based upon comparison with available experimental data, empirical correlations are obtained between the linear stability theory and the régimes in which: (i) the boundary layer is first noticeably oscillatory; (ii) the mean (temporal) flow quantities first deviate significantly from those of laminar flow.

1. Previous investigations

Since the interferometric study of Eckert & Soehngen (1951), considerable attention has been given to the stability of vertical natural convection boundary layers. The earliest analytical investigations in this field, those of Plapp (1957) and Szewczyk (1962), were based upon the asymptotic expansion technique (for large values of the Grashof number, G) which had previously been employed successfully in the stability of forced flow boundary layers. However, such theoretical results for the natural convection case were found to be incompatible with existing data, the theory predicting the flow to be much more stable than had been observed experimentally. This shortcoming of the asymptotic

† Present address: Clarkson College of Technology, Potsdam, New York.

expansion technique, combined with the complexity of such a procedure, indicated that here was a problem to be handled by a computer.

Kurtz & Crandall (1962) obtained the first numerical solutions, integrating the uncoupled disturbance vorticity equation by means of a finite-difference technique. Subsequently, Nachtsheim (1963) used a forward-integration technique and obtained solutions to the coupled vorticity and energy disturbance equations. He found that the buoyancy force arising from the temperature disturbance had a rather small effect upon the stability at a Prandtl number (σ) of 0·733, but a very significant destabilizing effect at $\sigma = 6{\cdot}7$. The results for $\sigma = 0{\cdot}733$ were corroborated by the hot-wire investigation in air performed by Colak-Antic (1964); however, the dye-trace data in water obtained by Szewczyk (1962) appeared to be in closer agreement with the uncoupled stability theory at $\sigma = 6{\cdot}7$. It was this latter result which led Sparrow, Tsou & Kurtz (1965) to assume that coupling could be neglected for large σ and, therefore, to study the $\sigma \to \infty$ limit with the disturbance temperature omitted. (It is shown in the present work that the coupled theory for $\sigma = 6{\cdot}7$ is compatible with the data of Szewczyk (1962) and others, and that the coupling effect is the prime source of instability for large σ.)

Although the above investigations concern an isothermal plate, the corresponding problem for a uniform-heat-flux plate was studied in the series of papers by Polymeropoulos & Gebhart (1967), Knowles & Gebhart (1968, 1969) and Dring & Gebhart (1968, 1969). The numerical results for this flow situation were found to be very similar to those of the isothermal plate when scaled in terms of the Grashof number (for a given σ); in addition, the analysis and computations of Knowles & Gebhart (1968) showed that the stability was significantly affected by a thermal capacity coupling between the wall and the fluid. By employing an interferometer and hot-wire probes, portions of the coupled neutral stability curve were determined for $\sigma = 0{\cdot}733$ and 6·7; it was found that these experimental results agreed with the theory, as did the measured disturbance temperature and velocity distributions normal to the plate, together with their rate of amplification in the streamwise direction.

Recently, Gill & Davey (1969) considered the stability of a 'buoyancy layer' (i.e. the one-dimensional flow arising from a doubly infinite, vertical plate heated to a uniform temperature excess relative to a linearly stratified external temperature field). They obtained coupled neutral curves numerically for a large range of σ (note: σ appeared only in the disturbance energy equation, the non-dimensionalized primary flow being independent of σ) and found the instability arising from coupling (or buoyancy) to be progressively more important with increasing σ. Based upon these results, they inferred the appropriate limiting process: $G = G(\sigma)$ as $\sigma \to \infty$, corresponding to the near-critical or nose region (i.e. the régime in G in which the flow is first unstable) of the buoyancy-driven mode, and proceeded to determine the first two terms in an asymptotic expansion for the disturbance field as $\sigma \to \infty$. In addition, they numerically solved the corresponding inviscid problem and substantiated the existence of an unstable wave-number (or frequency) band in the inviscid limit, as expected from the presence of an inflexion point in the primary velocity profile.

In the present paper, consideration is again given to the case of a uniform-heat-flux vertical plate. By using a numerical technique which is largely due to Mack (1965), coupled solutions are obtained for values of σ between 0·01 and 100 and for a much larger range of G than in former studies. In turn, these numerical solutions lead to some significant results which are enumerated in the present paper and its sequel (Hieber & Gebhart 1971, hereafter referred to as (B)) wherein asymptotic expansions are obtained for the limit $\sigma \to \infty$.

2. The governing equations

Considering the case of a uniform-heat-flux vertical plate, we employ the notation of Sparrow & Gregg (1956) and take the characteristic speed (U), length (δ) and temperature difference (ΔT) to be

$$U \equiv \frac{\nu}{5x} G^{*2}, \quad \delta \equiv \frac{5x}{G^*}, \quad \Delta T \equiv \frac{q\delta}{k} \quad \text{where} \quad G^* \equiv 5\left(\frac{g\beta q x^4}{5k\nu^2}\right)^{\frac{1}{5}}, \tag{1}$$

x being measured vertically upwards (the plate coinciding with the positive x axis), q being the uniform heat flux, ν the kinematic viscosity, k the thermal conductivity, β the coefficient of thermal expansion and g gravity. Applying the Boussinesq approximation and restricting attention to the boundary-layer region ($y = O(\delta) \ll O(x)$), we employ the standard procedure in linear stability theory of superimposing an arbitrarily small disturbance upon the primary flow such that the stream function and temperature distribution are of the form

$$\psi = (5\nu U x)^{\frac{1}{2}} [F(\eta) + \phi(\eta)\, e^{i(\gamma(x) - \omega t)}], \tag{2}$$

$$T - T_\infty = \Delta T [H(\eta) + \theta(\eta)\, e^{i(\gamma(x) - \omega t)}], \tag{3}$$

where physical quantities correspond to the real part of complex functions, $\eta \equiv y/\delta$ is the 'similarity' variable and

$$u = \partial\psi/\partial y, \quad v = -\partial\psi/\partial x,$$

(u, v) being the velocity components in the (x, y) directions and y the co-ordinate normal to the plate. Unless stated otherwise, the frequency ω will be taken to be real and γ to be complex (amplification of the disturbance therefore being spatial, corresponding to $d\gamma_i/dx < 0$).

In the limit η fixed as $G^* \to \infty$, the governing equations for the primary flow reduce to the boundary-layer equations

$$F''' + 4FF'' - 3F'F' + H = 0, \tag{4}$$

$$H'' + \sigma(4FH' - F'H) = 0, \tag{5}$$

subject to the boundary conditions

$$F'(\infty) = 0 = H(\infty) = F'(0) = F(0) = H'(0) + 1. \tag{6}$$

The governing equations for the disturbance field, as expressed in terms of the linearized vorticity and energy equations, assume the standard form

$$(F' - c)(\phi'' - \alpha^2\phi) - F'''\phi = \frac{1}{i\alpha G^*}(\phi^{\text{iv}} - 2\alpha^2\phi'' + \alpha^4\phi + \theta'), \tag{7}$$

$$(F'-c)\,\theta - H'\phi = \frac{1}{i\alpha\sigma G^*}(\theta''-\alpha^2\theta), \tag{8}$$

where $$\alpha \equiv \delta\, d\gamma/dx, \quad c \equiv \omega\delta/U\alpha.$$

The real part of α is the non-dimensionalized wave-number. Noting that $\alpha_i^2 \ll \alpha_r^2$, it follows that c_r is approximately equal to the non-dimensionalized phase speed.

Equations (7) and (8) are based upon the 'parallel mean flow' approximation of neglecting the algebraic x dependence of (2)–(3) [which includes the entire x dependence of the primary flow] relative to the exponential x dependence, $e^{i\gamma(x)}$. This follows from assuming that $|d\gamma/dx| = O(1/\delta)$ and noting that

$$x/\delta = O(G^*) > O(1)$$

in the boundary-layer régime.

By neglecting the algebraic x dependence of (2)–(3) in obtaining (7)–(8), some terms of $O(G^{*-1})$ have been omitted from the latter equations. However, these terms can be shown to involve lower-order derivatives than appear on the right-hand side of (7)–(8) and therefore may be neglected, the $O(G^{*-1})$ terms being significant only in those regions of the boundary layer in which the η derivatives of the disturbance field are large (in terms of G^*).

The boundary conditions for the disturbance field are

$$\phi(\infty) = 0 = \phi'(\infty) = \theta(\infty) = \phi(0) = \phi'(0) = \theta(0) \quad \text{or} \quad \theta'(0), \tag{9}$$

where the choice of the last condition in (9) depends upon the ability of the plate (in terms of its thermal capacity) to follow the temperature oscillation of the disturbance field. This coupling between the plate and the fluid results in an additional parameter (cf. Knowles & Gebhart 1968); for present purposes it is sufficient to consider the two limiting cases of a 'fast' oscillation (relative to the response time of the plate), for which $\theta(0) = 0$, and a 'slow' oscillation, for which $\theta'(0) = 0$.

It should be mentioned that the reason for employing the form $e^{i\gamma(x)}$, rather than the more standard $e^{i\gamma x}$, is that the precise x dependence of the exponent is not known *a priori*. In particular, Knowles & Gebhart (1969) have found experimentally that the disturbance wavelength grows approximately as $x^{\frac{3}{5}}$ for the case of a uniform-heat-flux plate. This result has been verified theoretically by Dring & Gebhart (1969) who found that, at fixed ω, the numerical value of c_r remains fairly constant as the disturbance moves downstream; due to the non-dimensionalization of c, this means that the phase speed and, hence, the wavelength are proportional to $x^{\frac{3}{5}}$. It is noted that the computed values of the current investigation are in agreement with the above results. In particular, the calculations indicate that the waves of maximum amplification are characterized by a wavelength and phase speed which are proportional to x^n where, for $\sigma = 0{\cdot}733$, n varies monotonically from approximately 0·65 to 0·75 in the G^* range of 200–1000 whereas, for $\sigma = 6{\cdot}7$, n lies between 0·56 and 0·58 in the G^* range from 100 to 1000 (to be compared with an experimental value of $0{\cdot}56 \pm 0{\cdot}04$ obtained by Knowles & Gebhart (1969) in a silicone oil of $\sigma = 7{\cdot}7$).

3. Some heuristic arguments

Nachtsheim (1963) has shown that the system (7)–(8) possesses three linearly independent integrals which vanish at infinity. Denoting these integrals as $(\phi_1, \theta_1), (\phi_2, \theta_2), (\phi_3, \theta_3)$, they may be chosen such that, as $\eta \to \infty$,

$$\left.\begin{aligned} &\phi_1 \sim e^{-\alpha\eta}, \quad \sigma_2 \sim e^{-\alpha_2\eta}, \quad \phi_3 \sim e^{-\alpha_3\eta}, \\ &\theta_1 \sim i\alpha\sigma G^* H'\phi_1/(\alpha^2 - i\alpha c\sigma G^* - (\alpha + 4\sigma F_\infty)^2), \\ &\theta_2 \sim i\alpha\sigma G^* H'\phi_2/(\alpha^2 - i\alpha c\sigma G^* - (\alpha_2 + 4\sigma F_\infty)^2), \\ &\theta_3 \sim (\alpha_3^2 - \alpha^2 + i\alpha c G^*)(\alpha_3^2 - \alpha^2)\,\phi_3/\alpha_3, \end{aligned}\right\} \tag{10}$$

where $\alpha_2 \equiv [\alpha^2 - i\alpha c G^*]^{\frac{1}{2}}$, $\alpha_3 \equiv [\alpha^2 - i\alpha c\sigma G^*]^{\frac{1}{2}}$ (with $\alpha_{2r}, \alpha_{3r} > 0$) and

$$H' \sim -A\, e^{-4\sigma F_\infty \eta}$$

(with $F_\infty \equiv \lim_{\eta\to\infty} F(\eta)$ and A being positive constants). Therefore, the solution to (7)–(9) is expressible as

$$\phi = \phi_1 + B_2\phi_2 + B_3\phi_3, \quad \theta = \theta_1 + B_2\theta_2 + B_3\theta_3, \tag{11}$$

where the coefficient of ϕ_1 has been chosen to be unity, thereby fixing the arbitrary scale of the disturbance level.

Ostrach (1964) has shown that (ϕ_1, θ_1) is associated with the inviscid limit and that (ϕ_2, θ_2), (ϕ_3, θ_3) are characterized, respectively, by the exponential behaviours

$$\exp\left(-\int^\eta [i\alpha G^*(F' - c)]^{\frac{1}{2}}\, d\eta\right), \quad \exp\left(-\int^\eta [i\alpha\sigma G^*(F' - c)]^{\frac{1}{2}}\, d\eta\right). \tag{12}$$

For convenience, we will denote $(\,)_1$, $(\,)_2$, $(\,)_3$ as the inviscid, the viscous uncoupled and the viscous coupled integrals ('coupling' referring to the dependence of the disturbance velocity upon the θ field via the buoyancy term in (7)). Of immediate interest are the following properties of these integrals:

$$\left.\begin{aligned} &\frac{d}{d\eta}(\,)_1 = O(1), \quad \frac{d}{d\eta}(\,)_2 = O(G^{*\frac{1}{2}}) = \frac{d}{d\eta}(\,)_3, \\ &\theta_1/\phi_1 = O(1) = \theta_2/\phi_2, \quad \theta_3/\phi_3 = O(G^{*\frac{3}{2}}), \end{aligned}\right\} \tag{13}$$

where we are considering α and σ to be fixed as $G^* \to \infty$. The indicated properties of $(\,)_1$ are applicable except within the two 'critical' layers, of $O(G^{*-\frac{1}{3}})$ in thickness, which need not concern us provided c_r is bounded away from zero, assuring that such layers are removed from the wall; the last relation in (13) arises from the fact that $(\,)_3$ is associated with a zeroth-order coupling effect, the term $\theta_3'/i\alpha G^*$ effectively behaving as a forcing function in (7).

Based upon (11) and (13), some important conclusions can be drawn concerning the behaviour of the disturbance field as $G^* \to \infty$. Considering α to be specified and c to be the eigenvalue, we turn first to the inviscid problem (denoting the corresponding eigenvalue and eigenfunction with a superscript tilde):

$$L(\tilde{\phi}; \tilde{c}) \equiv (F' - \tilde{c})(\tilde{\phi}'' - \alpha^2\tilde{\phi}) - F'''\tilde{\phi} = 0; \quad \tilde{\phi} = 0 \quad \text{at} \quad \eta = 0, \infty. \tag{14}$$

Since F' and F'''' are exponentially small as $\eta \to \infty$, it follows that $\tilde{\phi} = \tilde{\phi}_1$ (where $L(\tilde{\phi}_1; \tilde{c}) = 0$ and $\tilde{\phi}_1 \sim e^{-\alpha\eta}$ as $\eta \to \infty$) with $\tilde{c} = \tilde{c}(\alpha)$ chosen such that $\tilde{\phi}_1(0) = 0$.

Denoting the corresponding uncoupled (Orr-Sommerfeld) problem with a superscript caret, we have:

$$L(\hat{\phi}; \hat{c}) = \frac{1}{i\alpha G^*}(\hat{\phi}^{\mathrm{iv}} - 2\alpha^2\hat{\phi}'' + \alpha^4\hat{\phi}); \quad \hat{\phi} = 0 = \hat{\phi}' \quad \text{at} \quad \eta = 0, \infty. \tag{15}$$

If we were to take $\hat{c} = \tilde{c}$, we would then have

$$\hat{\phi}_1 = \tilde{\phi}_1 + O(G^{*-1}),$$

resulting in $\hat{\phi}_1(0) = O(G^{*-1})$, $\hat{\phi}_1'(0) = O(1)$. However, since $\hat{\phi}_2'(0)/\hat{\phi}_2(0) = O(G^{*\frac{1}{2}})$, it follows that, with $\hat{c} = \tilde{c}$, the function

$$\hat{\phi} = \hat{\phi}_1 + \hat{B}_2\hat{\phi}_2$$

can satisfy the condition $\hat{\phi}'(0) = 0$ by a proper choice of $\hat{B}_2$ but $\hat{\phi}(0)$ will remain non-zero, of $O(G^{*-\frac{1}{2}})$. Hence, noting that

$$\frac{\partial}{\partial c}(\ )_1 = O(1), \quad \frac{\partial}{\partial c}\log(\ )_2 = O(G^{*\frac{1}{2}}), \tag{16}$$

we are led to the well-known result (cf. Morawetz 1952):

$$\hat{c}(\alpha, G^*) = \tilde{c}(\alpha) + O(G^{*-\frac{1}{2}}). \tag{17}$$

Turning now to (7)–(9), we first consider the case $\theta(0) = 0$. If we assume that $c = \hat{c}$ and $B_2 = \hat{B}_2$, it then follows from (8) and (13) that, neglecting terms of $O(G^{*-1})$,

$$\theta_1(0) = \frac{H'(0)}{F'(0) - \hat{c}}\hat{\phi}_1(0) = O(G^{*-\frac{1}{2}}),$$

$$B_2\theta_2(0) = \left(\frac{\sigma}{1-\sigma}\right)\frac{H'(0)}{F'(0) - \hat{c}}\hat{B}_2\hat{\phi}_2(0) = O(G^{*-\frac{1}{2}}).$$

(It is assumed that $\sigma \neq 1$.) In order that $\theta(0) = 0$, it is then necessary that $B_3\theta_3 = O(G^{*-\frac{1}{2}})$ in the region near the wall, indicating (on the basis of (13)) that the contribution of $(\ )_3$ to $\phi(0)$ and $\phi'(0)$ is of $O(G^{*-2})$ and $O(G^{*-\frac{3}{2}})$, respectively. In addition, still assuming that $c = \hat{c}$, we have

$$\phi_1 = \hat{\phi}_1 + O(G^{*-1}), \quad \phi_2 = (1 + O(G^{*-1}))\,\hat{\phi}_2,$$

where the terms of $O(G^{*-1})$ arise from the coupling term in (7). Therefore, with $c = \hat{c}$ and $B_2 = \hat{B}_2$, the conditions $\phi(0) = 0 = \phi'(0)$ are satisfied to $O(G^{*-1})$. Resorting again to (16), we are led to the result:

$$c(\alpha, G^*) = \hat{c}(\alpha, G^*) + O(G^{*-1}). \tag{18}$$

For the case $\theta'(0) = 0$, one finds that $B_3\theta_3'(0) = O(1)$; the remainder of the argument proceeds as above. Hence, (18) applies in this case also.

We note that, whereas $(\ )_2$ is a viscous boundary layer (corresponding to the region $\eta = O(G^{*-\frac{1}{2}})$) which is required in order to cancel the slip associated with $(\ )_1$, $(\ )_3$ is a thermal boundary layer which is required in order to satisfy the temperature boundary condition at $\eta = 0$. Of prime importance in this last regard is the property that $(\ )_3$ is effectively a temperature disturbance, the associated velocity being smaller by $O(G^{*-1})$.

It is to be noted that the above heuristic argument leading to (18) is essentially equivalent to a method employed by Ostrach & Maslen (1961) in analyzing the stability of natural convection channel flow. However, in relating their results to the stability of natural convection boundary layers, the above authors, in effect, took the wavelength to be $O(x)$ rather than $O(\delta)$, and were thereby led to the erroneous conclusion that coupling is a zeroth-order effect as $G^* \to \infty$.

In particular, the results in (17) and (18) indicate that, as $G^* \to \infty$, the effect of coupling vanishes more rapidly than that of viscosity. This is borne out in the numerical results presented in the next section.

4. Some numerical solutions

The results of the present section are based upon a numerical procedure which is significantly simpler than those previously employed on this problem. Basically, the method is the same as that employed by Mack (1965) in his stability analysis of the compressible forced flow boundary layer.

As was done by Dring & Gebhart (1968), we integrate in from the edge of the boundary layer, employing the form indicated in equation (11). However, unlike the previous analysis, we do not assume the values of B_2 and B_3 but rather integrate ϕ_1, ϕ_2 and ϕ_3 separately. Specifically, for given real values of G^* and $\omega\delta/U$, we guess a complex value for α(note: $c = \omega\delta/U\alpha$) and, starting with (10) as initial values for the integrals, employ a fourth-order Runge–Kutta method in order to integrate (7)–(8) across the boundary layer. Obtaining the values of the integrals at the wall, we determine B_2 and B_3 by applying two of the boundary conditions at $\eta = 0$; the remaining boundary condition, $\theta(0) = 0$, say, is satisfied only if α takes on an appropriate value (eigenvalue) for the given G^* and $\omega\delta/U$. Typically, the value of α must be determined via an iterative process. For example, if the assumed value of α results in $\theta(0) = \chi \neq 0$, the value of α is then changed slightly to $\alpha + \Delta\alpha_r$ and the integration repeated, resulting in $\theta(0) = \chi + \Delta\chi$, say. Employing the Cauchy–Riemann relations ($\partial\theta_r(0)/\partial\alpha_r = \partial\theta_i(0)/\partial\alpha_i$, etc.) and approximating partial derivatives with finite differentials ($\partial\theta_r(0)/\partial\alpha_r \approx \Delta\chi_r/\Delta\alpha_r$, etc.), an improved value for α is readily obtained via a simple linear extrapolation. This process is then repeated successively until $|\theta(0)|$ is sufficiently small ($\leqslant 10^{-4}$, typically).

The simplification of the present technique is apparent: rather than guessing the value of three complex numbers (as in the methods of Nachtsheim (1963) and Dring & Gebhart (1968)), only the value of α must be assumed. Hence, the problem is reduced to finding a point in two-dimensional rather than six-dimensional space. This simplification is particularly advantageous as G^* increases since, due to parasitic growth (see Kaplan 1964 or Betchov & Criminale 1967) in the numerically determined $(\ )_1$, the value of B_2 or B_3 rapidly increases. In fact, unless a purification scheme such as that of Kaplan (1964) were employed, any forward-integration procedure would be limited in G^* by the size of B_2 or B_3 relative to the number of significant figures available to the computer (e.g. with 16 significant figures, the method would break down as B_2 or B_3 approached 10^{16}).

The results presented below are based upon the above technique with the

mesh size (h) and boundary-layer edge (η_e) chosen in order to minimize computer time and still assure adequate accuracy (typically, α_r and α_i are correct to within 0·1 and 1 %, respectively). For example, the calculations for $\sigma = 0{\cdot}733$ are based upon $h = 0{\cdot}1$ and $\eta_e = 5$; for $\sigma = 100$, $\eta_e = 14$ with $h = 0{\cdot}1$ for $\eta < 2$ and $h = 0{\cdot}2$ for $\eta > 2$; for $\sigma = 0{\cdot}01$, $\eta_e = 20$ with $h = 0{\cdot}1$ for $\eta < 1$ and $h = 0{\cdot}2$ for $\eta > 1$. (The use of two mesh sizes in the case of extreme values of σ is a consequence of the two-layer structure which the primary flow exhibits as either $\sigma \to 0$ or $\sigma \to \infty$).

All computations were performed in double precision on an I.B.M. 360/65. In some cases, the above method was supplemented with the purification scheme of Kaplan (1964). Specifically, purification was employed in obtaining the large G^* portion of the uncoupled neutral curve for $\sigma = 0{\cdot}733$ (figure 6), the results (other than in the near-critical region) for $\sigma = 0{\cdot}025$ (figure 8(*b*)) and $\sigma = 0{\cdot}01$ (figure 8(*c*)), and the coupled neutral curve in the large G^* portion of figure 8(*e*) [$\sigma = 6{\cdot}7$]. In the first of these cases, the purification was exactly the same as that employed by Kaplan (1964), $(\,)_1$ being adjusted at each mesh point (by the addition of an appropriate multiple of $(\,)_2$) such that

$$(F'-c)(\phi_1''-\alpha^2\phi_1)-F'''\phi_1 = 0.$$

For the cases $\sigma = 0{\cdot}025$ and $\sigma = 0{\cdot}01$, both $(\,)_1$ and $(\,)_3$ were corrected relative to $(\,)_2$ [$(\,)_2$ being the most rapidly increasing integral (as η decreases) when $\sigma < 1$, see equation (12)], $(\,)_1$ being purified according to the above inviscid relation and $(\,)_3$ being adjusted such that

$$\theta_3''-i\alpha\sigma G^*(F'-c)\,\theta_3 = 0.$$

In the case $\sigma = 6{\cdot}7$, $(\,)_1$ and $(\,)_2$ were purified relative to $(\,)_3$, $(\,)_1$ being corrected according to the above inviscid relation and $(\,)_2$ being adjusted so that

$$\phi_2^{\mathrm{iv}}-i\alpha G^*(F'-c)\,\phi_2'' = 0.$$

4.1. *Prandtl number of* 0·733

For $\sigma = 0{\cdot}733$, the contours of constant α_i corresponding to amplification ($\alpha_i < 0$) and neutral stability ($\alpha_i = 0$) are shown in figures 1 and 2 for the conditions $\theta(0) = 0$ and $\theta'(0) = 0$, respectively. In each case, the neutral curve exhibits the characteristic 'nose' first obtained by Nachtsheim (1963). For the first time, however, it is seen in figure 2 that there exists a loop in the neutral stability curve for the case $\theta'(0) = 0$. (The results obtained by Knowles & Gebhart 1968 for this case were curtailed at $G^* \approx 180$, i.e. just before the looping region.) In fact, the case $\theta(0) = 0$ has a similar loop which, however, occurs in the damped region and therefore does not appear in figure 1. As will be shown immediately, these loops arise from a merging of two sets of eigenvalues in the $(G^*, \omega\delta/U)$ plane.

In order to study the details of the loop structure, the contours of constant α_i are presented in figure 3 for the loop region for the case $\theta(0) = 0$. The two indicated families of curves are related as follows. Starting at A and making a traverse along the rectangular contour $ABCD$ or any other closed contour

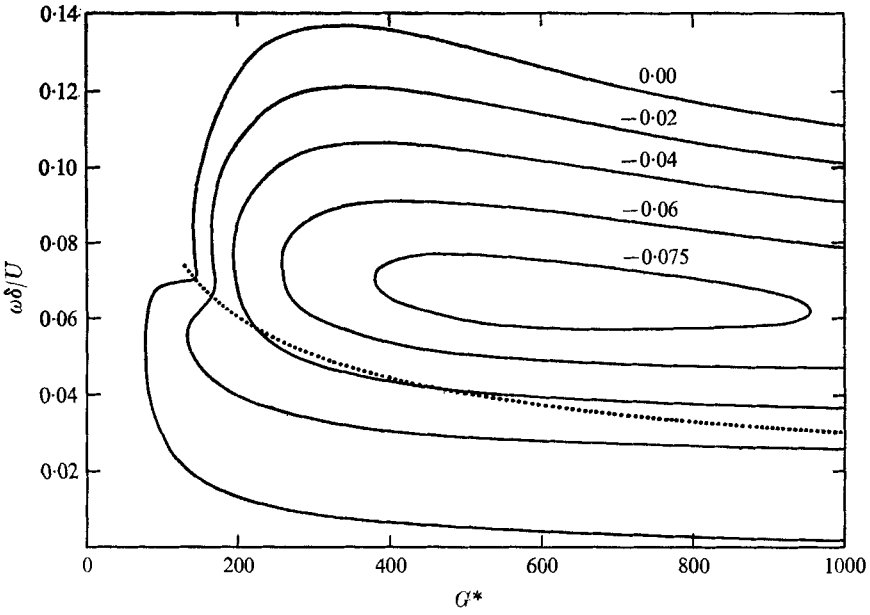

FIGURE 1. Contours of constant $\alpha_i (\leqslant 0)$ for $\sigma = 0{\cdot}733$, $\theta(0) = 0$. Dotted curve is 'branch cut'.

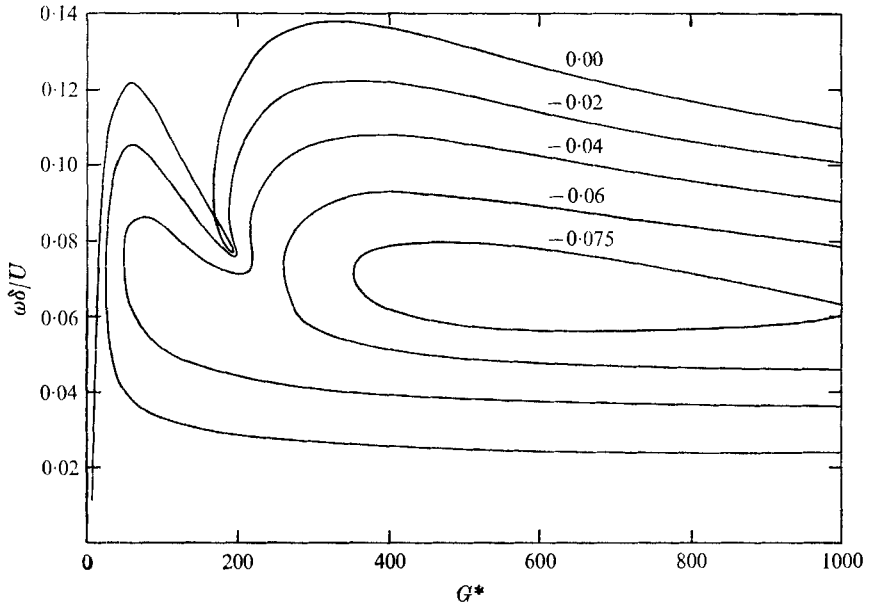

FIGURE 2. Contours of constant $\alpha_i (\leqslant 0)$ for $\sigma = 0{\cdot}733$, $\theta'(0) = 0$.

enclosing any of the constant α_i loops, α_i varies continuously but does not return to its original value upon arriving at A; rather, α_i assumes the value associated with the other family. Following a second traverse, the original value of α_i is recovered. On the other hand, in traversing the rectangular contour $AEFD$ or any other closed contour not containing any of the constant α_i loops, the original value of α_i is obtained each cycle. It follows that, with regard to the behaviour of α_i in the $(G^*, \omega\delta/U)$ plane, there exists a point P which is common to the interior of all the constant α_i loops and which, in effect, is a branch point of the first order.

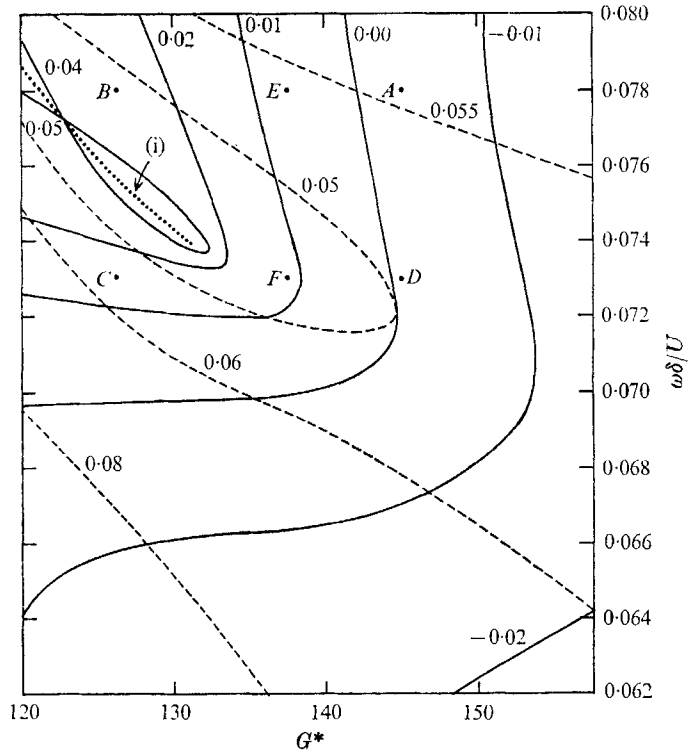

FIGURE 3. 'Loop region': contours of constant α_i for $\sigma = 0{\cdot}733$, $\theta(0) = 0$. Curve (i) is locus of points at which α_i is the same for both modes.

Corresponding contours of constant α_r, presented in figure 4, indicate the existence of constant α_r loops in the same region of the $(G^*, \omega\delta/U)$ plane. With curve (i) in figure 3 being the locus of points at which α_i is the same for both 'branches' (or modes), and curve (ii) in figure 4 the corresponding curve for α_r, it is seen that P must be the intersection point of (i) and (ii); that is, P is the point where the two values of α coalesce. (It is tacitly assumed that any other sets of eigenvalues which may exist will be highly damped throughout the $(G^*, \omega\delta/U)$ plane.) In order to clearly define the two modes, we choose to consider a 'branch cut' from P along curve (ii) and identify mode I with the branch having a negative α_i at point A. Hence, mode I includes the upper portion of the amplified region in figure 1 whereas mode II contains the nose region. The cut is shown as a

dotted line in figure 1. For all other subsequent cases for which this bi-modal structure exists, the modes are to be identified in terms of a similar cut.

It should be noted that Nachtsheim (1963) recognized that the nose portion of the neutral stability curve actually corresponded to a second mode. However, he did not obtain two sets of eigenvalues. Recently, Gill & Davey (1969), in their stability analysis of a 'buoyancy layer', did obtain two sets of eigenvalues. They did not, however, pursue the matter of relating these modes and, as a result, did not discover any loops.

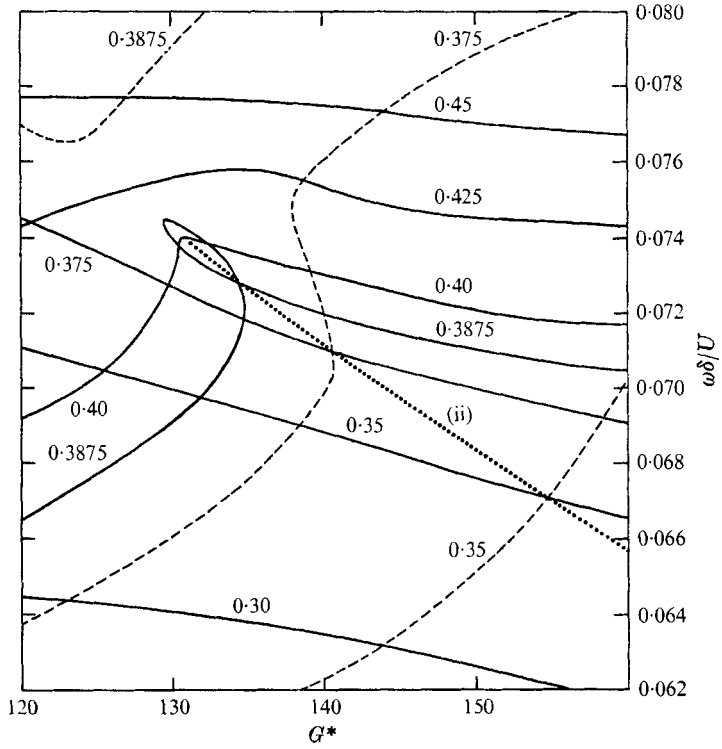

FIGURE 4. 'Loop region': contours of constant α_r for $\sigma = 0{\cdot}733$, $\theta(0) = 0$. Curve (ii) is locus of points at which α_r is the same for both modes.

By comparing figures 1 and 2 in the large G^* portion, it is seen that both cases appear to approach the same asymptotic behaviour. Making comparison with the corresponding uncoupled results of figure 5, it is clear that the coupled stability characteristics for either $\theta(0) = 0$ or $\theta'(0) = 0$ approach those of the uncoupled problem as $G^* \to \infty$; this is in agreement with §3 where, according to equation (18), the coupling effect vanishes as $O(G^{*-1})$.

In order to examine the stability problem for extremely large G^*, it follows that it is sufficient to consider the uncoupled case. This has been done in figure 6 where the upper portion of the uncoupled neutral curve for $\sigma = 0{\cdot}733$ is presented for values of G^* out to 18000. The behaviour of the curve is peculiar in that it is oscillatory but does seem to approach a definite limit.

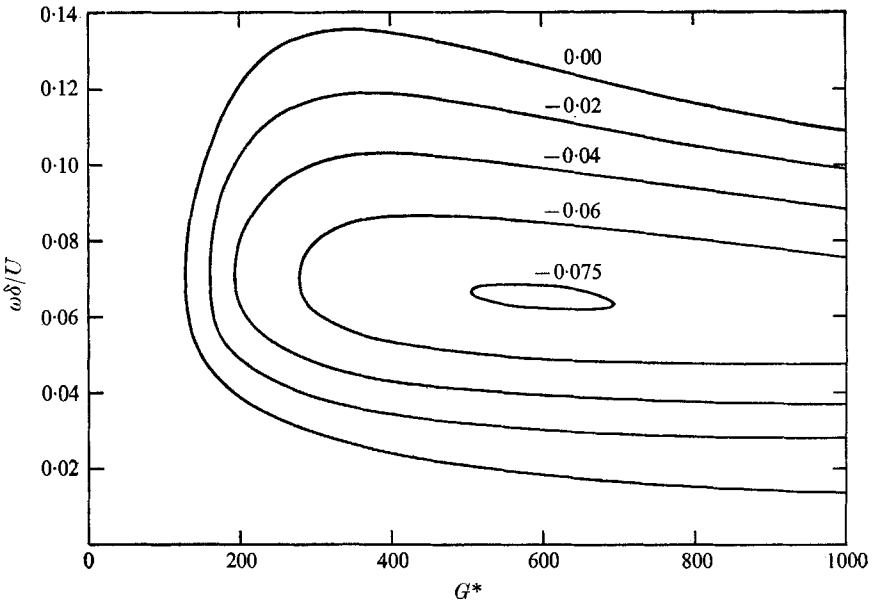

FIGURE 5. Contours of constant α_i ($\leqslant 0$) for $\sigma = 0{\cdot}733$, uncoupled.

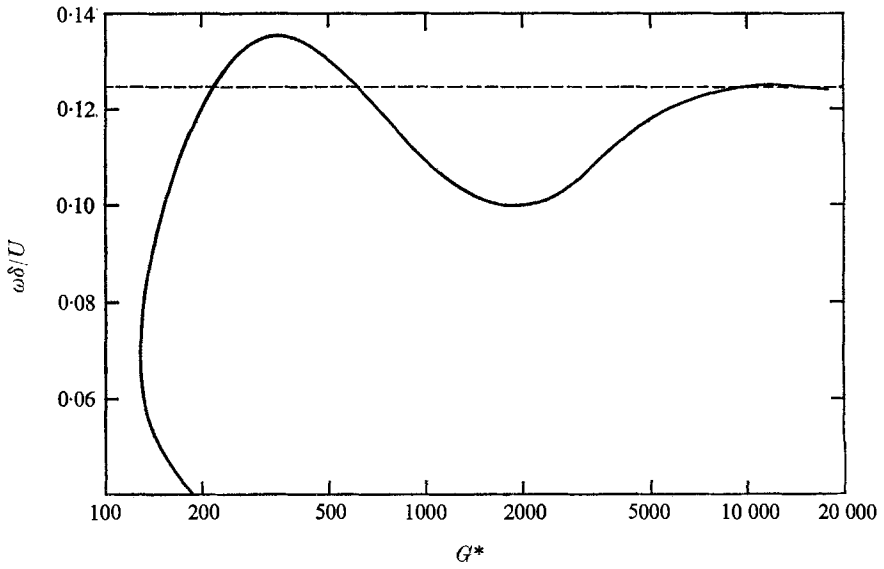

FIGURE 6. Upper portion of uncoupled neutral curve for $\sigma = 0{\cdot}733$. Dashed line corresponds to neutral stability in inviscid limit.

In order to identify the latter limit, we solved the corresponding inviscid problem (integrating in the complex η plane along the path indicated at the top of figure 7) and determined the frequency at which the inviscid flow is neutrally stable; this is indicated as a dashed line in figure 6. Hence, the uncoupled (and, on the basis of previous results, the coupled) problem is seen to be asymptotic to the inviscid case as $G^* \to \infty$. In addition, the coupling effect is seen to vanish more rapidly than that of viscosity; this is in agreement with §3, (17) and (18).

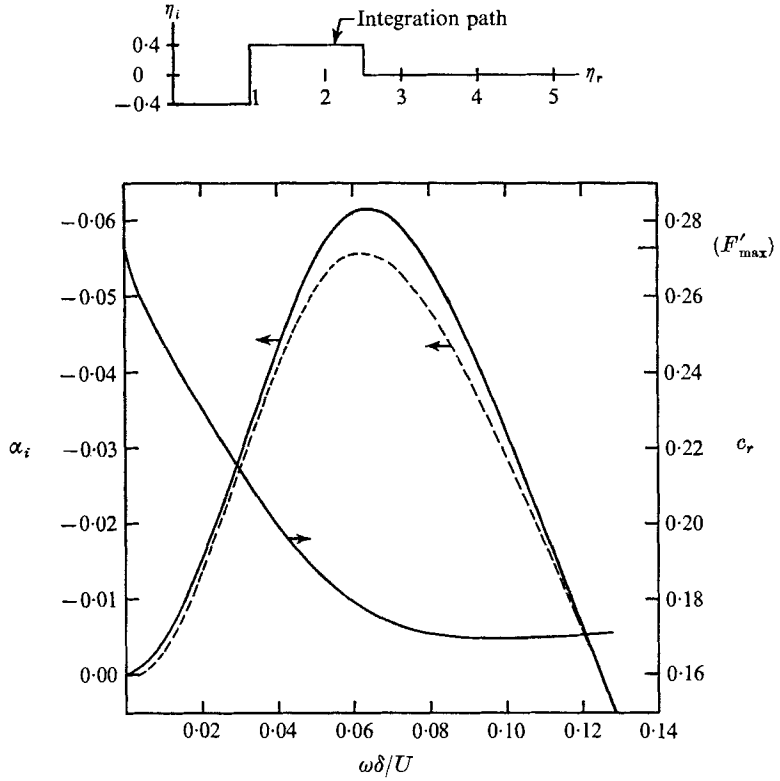

FIGURE 7. Inviscid limit for $\sigma = 0{\cdot}733$. Dashed curve is uncoupled result at $G^* = 10000$.

Additional results for the inviscid problem are indicated in figure 7. For comparison, the uncoupled results for α_i at $G^* = 10000$ are indicated as a dashed curve. It is noted that $c_r \to F'_{\max}$ as $\omega\delta/U \to 0$ (cf. Drazin & Howard 1962 or Gill & Davey 1969); on the other hand, the value of c_r at the upper neutral point does not appear to have any particular significance. (One might expect it to equal the base flow speed at the inflexion point, F'_{infl}, thereby eliminating one of the critical points; such is not the case, however, since $F'_{\text{infl}} \approx 0{\cdot}193$.)

4.2. *Small Prandtl number fluids*

Restricting attention to the case $\theta(0) = 0$, the constant $\alpha_i (\leqslant 0)$ contours are presented in figures 8(*a*), (*b*) and (*c*) for $\sigma = 0{\cdot}1$, $0{\cdot}025$ and $0{\cdot}01$, respectively. For comparison, the uncoupled neutral curves are indicated as dashed contours.

It is immediately evident that, for this range of σ, the neutral stability curve is only weakly dependent upon the coupling effect and upon σ. On the other hand, it is noted that the maximum value of $-\alpha_i$ decreases rather rapidly as σ decreases. In addition, unlike the above results for $\sigma = 0{\cdot}733$, it is seen that there is only one mode in each of these small Prandtl number cases.

Hence, on the basis of these three values of σ, it would appear that, for small σ, the stability characteristics are fairly well approximated by those of the uncoupled problem with the flow rapidly becoming less unstable as σ decreases. In particular, we would therefore expect the neutral curve for $\theta'(0) = 0$ to be quite similar to those for the uncoupled and $\theta(0) = 0$ cases. Such, however, is not the case, as was discovered by determining the former curve for $\sigma = 0{\cdot}1$ (shown as dotted contour in figure 8(*a*)). Although the boundary-layer régime does not actually correspond to such small values of G^*, the dotted curve in figure 8(*a*) does imply that the boundary layer is markedly unstable when $\theta'(0) = 0$. Hence, the results presented in figures 8(*a*)–(*c*) suggest that, for extremely small σ, coupling is rather negligible when $\theta(0) = 0$ but has a significantly destabilizing effect when $\theta'(0) = 0$.

4.3. *Large Prandtl number fluids*

Results for the case $\theta(0) = 0$ are presented in figures 8(*d*)–(*g*) for $\sigma = 2{\cdot}5, 6{\cdot}7, 25, 100$. (The last two curves are limited in G^* due to the large growth of $(\ )_3$ across the boundary layer – of the order of 10^{80}, the upper limit of the computer.) It is immediately evident that mode II becomes the predominant source of instability as σ becomes large. In particular, from figures 8(*d*) and (*e*) it appears that the unstable region corresponding to mode I is always contained by that of the uncoupled problem; the uncoupled neutral curves in figures 8(*f*) and (*g*) then imply that the critical G^* of mode I rapidly increases with σ. (It is to be noted that the paper by Sparrow *et al.* (1965) is restricted to the uncoupled problem. Therefore, at best, their results could be used to describe mode I of the coupled problem.) On the other hand, the critical G^* of mode II appears to reach a minimum at $\sigma \approx 25$ and to slowly increase with larger values of σ. In addition, as σ increases, the non-dimensionalized frequencies corresponding to the nose region of II are seen to become conspicuously larger than those of I or the associated uncoupled mode, suggesting the existence of two distinct characteristic frequencies as $\sigma \to \infty$. This matter is considered in detail in (B).

For comparison, the neutral stability curve for $\theta'(0) = 0$ has been indicated in figure 8(*g*) for $\sigma = 100$. The similarity in the neutral curves for $\theta(0) = 0$ and $\theta'(0) = 0$ suggest that, as $\sigma \to \infty$, the stability characteristics become independent of the thermal capacity of the plate. This is proved in (B).

5. Transition to turbulence: comparison of theory and experiment

The purpose of the present section is to establish correlations between the above theoretical results and some of the experimentally determined flow régimes which comprise the turbulent-transition process. For the sake of convenience,

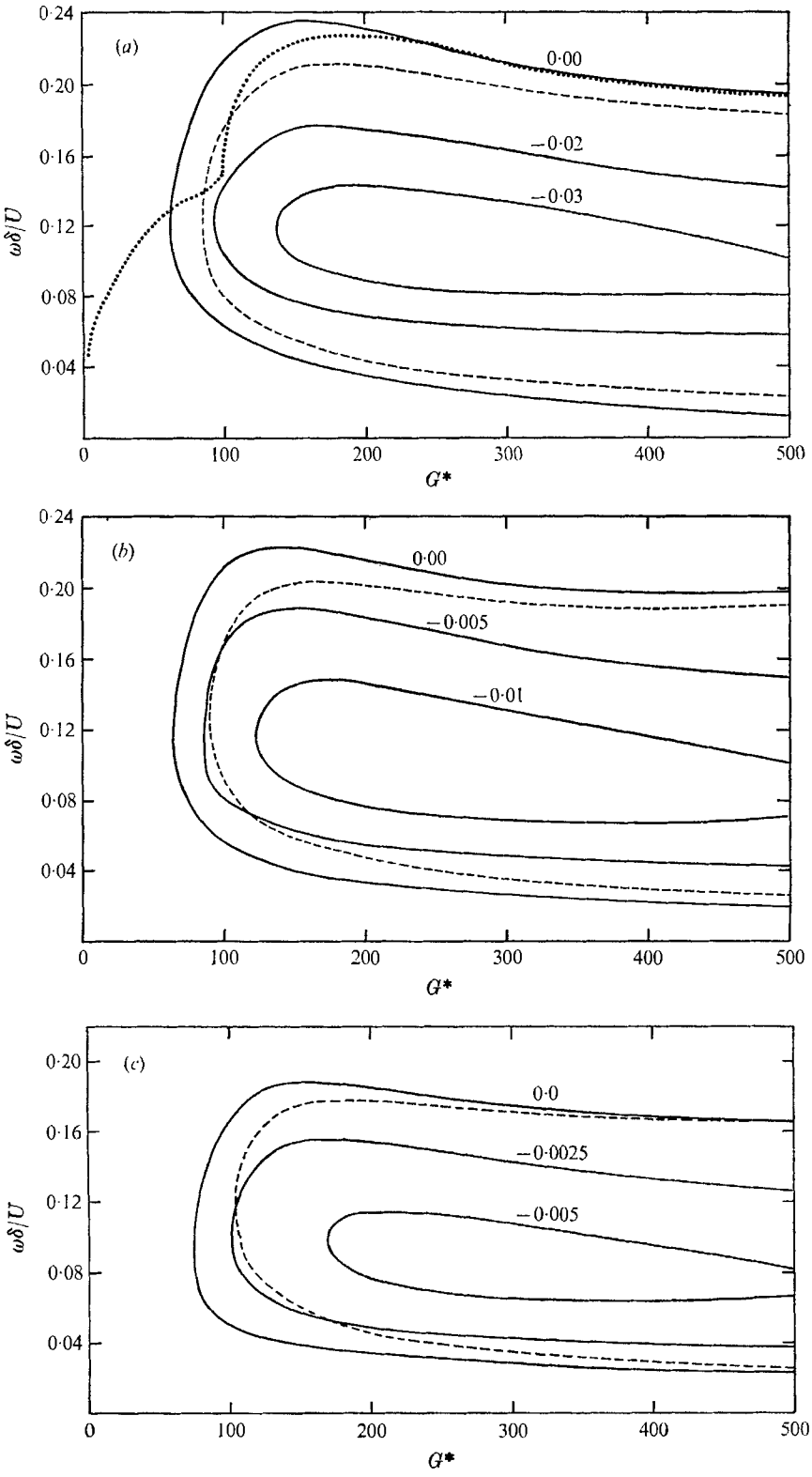

FIGURE 8. For legend see p. 641.

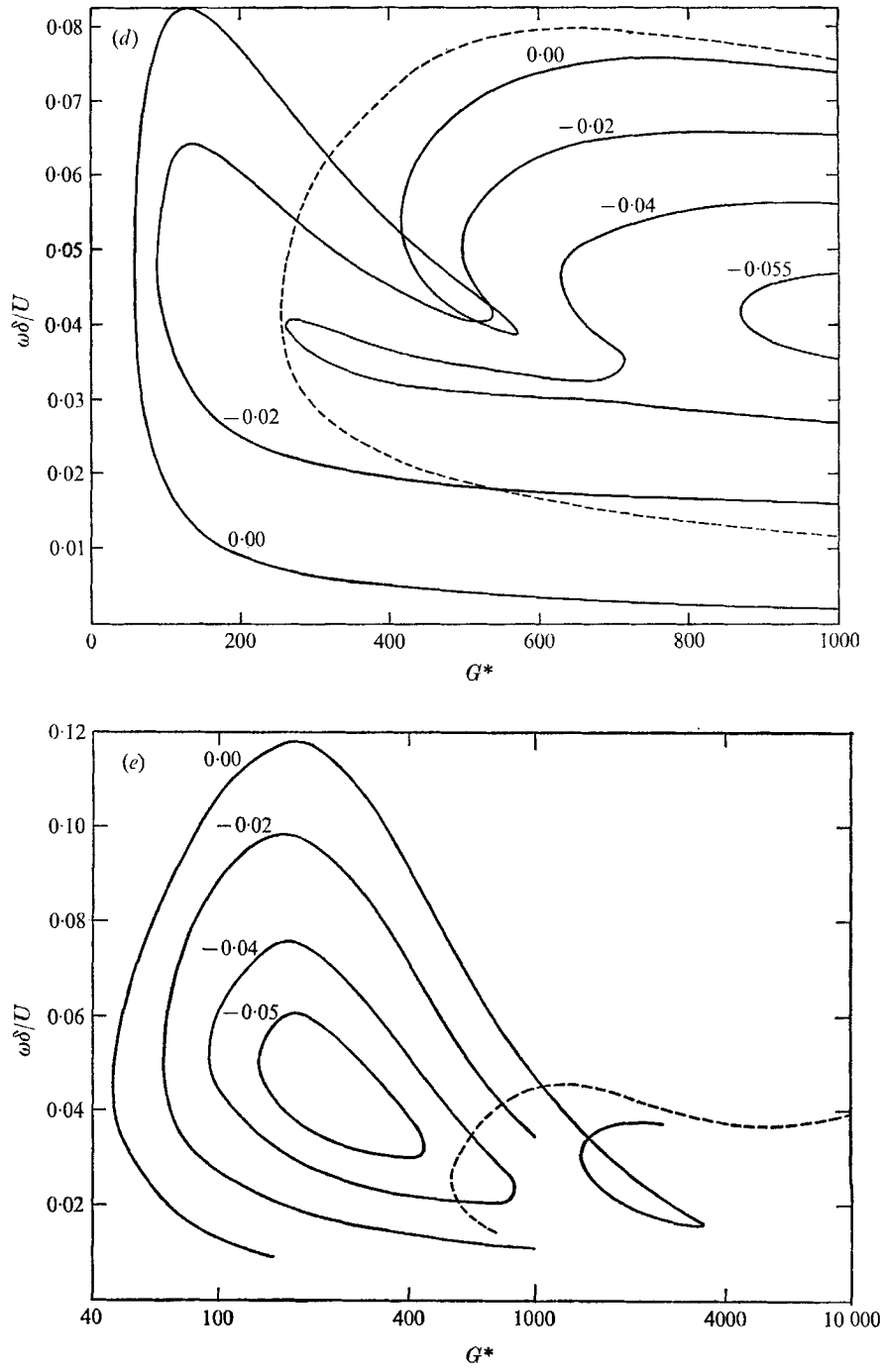

FIGURE 8. For legend see facing page.

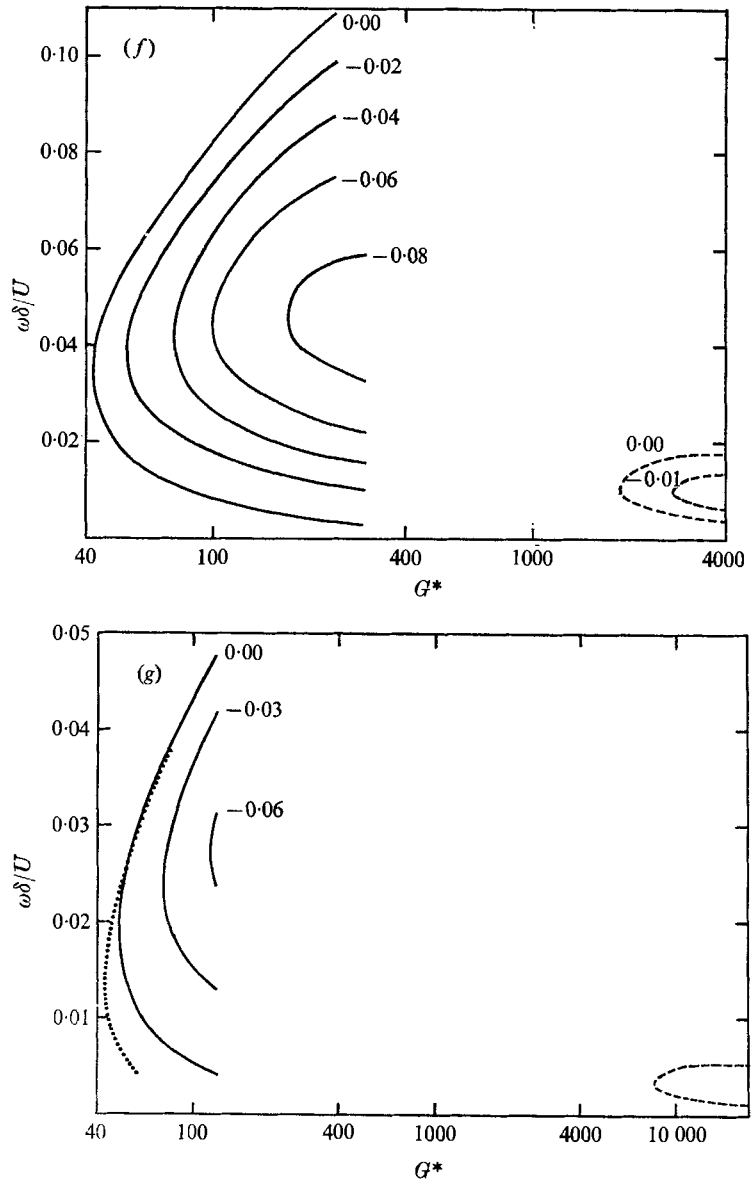

FIGURE 8. Contours of constant α_i ($\leqslant 0$) for $\theta(0) = 0$. Dashed line is uncoupled neutral curve; dotted curve is neutral curve for $\theta'(0) = 0$. (*a*) $\sigma = 0{\cdot}1$; (*b*) $\sigma = 0{\cdot}025$; (*c*) $\sigma = 0{\cdot}01$; (*d*) $\sigma = 2{\cdot}5$; (*e*) $\sigma = 6{\cdot}7$; (*f*) $\sigma = 25$; (*g*) $\sigma = 100$.

we focus attention on the régimes in which: (i) the boundary layer is first noticeably oscillatory; and (ii) the mean (temporal) flow quantities first deviate significantly from those of laminar flow. We will arbitrarily denote the latter régime as the 'onset of turbulence'. (In the case of the uniform-flux plate, (ii) corresponds to the stage at which the local mean wall temperature first deviates markedly from the $x^{\frac{1}{5}}$ dependence of the laminar régime.) Clearly, (ii) is a régime wherein the non-linear interaction between the oscillations cannot be ignored,

indicating that linear stability theory is no longer applicable. However, by comparing the above theoretical results with pertinent data, it is hoped that some empirical correlation can be established between the results of linear stability theory and the onset of turbulence.

Such a correlation does exist for boundary layers in forced flow, Smith (1957) having shown that, provided the free stream is of sufficiently small turbulent intensity, the transition 'point' corresponds to the Reynolds number at which max $(\int \omega_i dt) \approx 9$, where: ω_i is the imaginary part of the frequency (temporal amplification) as determined from linear stability theory; the integration is along constant frequency (ω_r) paths (describing the propagation of disturbance waves) from the neutral stability curve to the given Reynolds number; the maximization is with respect to all constant frequency paths. In the present case (spatial amplification), the corresponding integral, denoting the exponential growth of the disturbance field, is $-\frac{1}{4}\int \alpha_i dG^*$ (cf. Dring & Gebhart 1968), where the integration is as above.

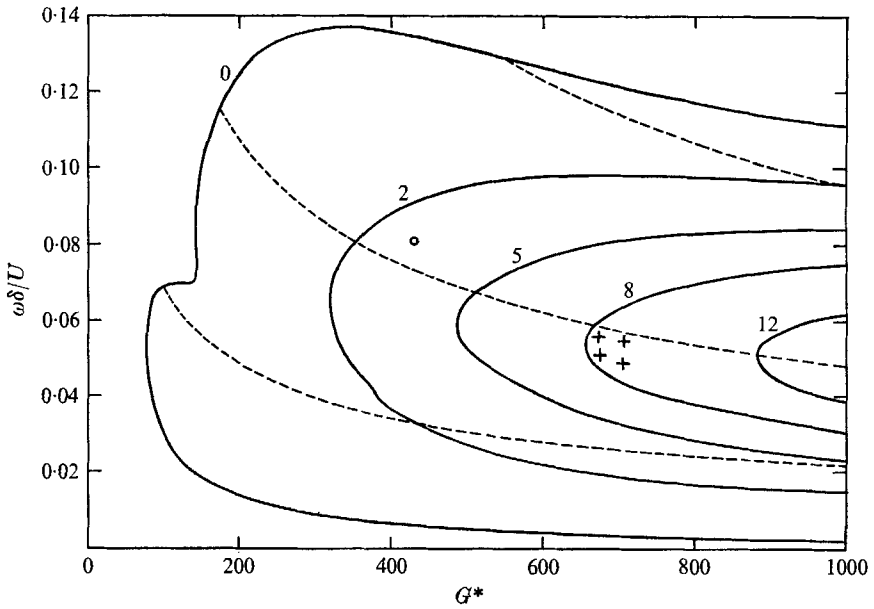

FIGURE 9. Contours of constant $-\frac{1}{4}\int \alpha_i dG^*$ for $\sigma = 0{\cdot}733$, $\theta(0) = 0$. Dashed curves are constant frequency paths. Data: ○, Eckert & Soehngen (1951); +, Polymeropoulos (1966).

The calculated spatial amplification characteristics of Dring & Gebhart (1968), when combined with the paths followed on the stability plane by constant frequency disturbances as they are convected downstream, indicate that the present natural convection flow highly favours a narrow band of frequencies for amplification. In a recent review of such instability, Gebhart (1969) has analyzed the available experimental indications, in gases and water, of the first local appearance of highly amplified disturbances and/or transition arising from 'natural' or 'random' disturbances; all points, when converted to the co-ordinates of the stability plane, were found to lie in the portion of the unstable region of

highest amplification rate. The present results assess this correspondence in terms of more complete results from stability theory.

Contours of constant values of the exponential growth factor, $-\frac{1}{4}\int \alpha_i dG^*$, are presented in figures 9 and 10 for the cases $\sigma = 0{\cdot}733$, $\theta(0) = 0$ and $\sigma = 6{\cdot}7$, $\theta(0) = 0$; the dashed curves correspond to fixed values of ω, denoting the propagation of disturbance waves in the stability plane (note $G^* \sim x^{\frac{1}{2}}$ whereas, for ω constant, $\omega\delta/U \sim x^{-\frac{3}{8}}$). It should be observed that corresponding plots for $\theta'(0) = 0$ would not be significantly different, at least in the range $G^* \gtrsim 500$ [compare figure 1 with 2 and figure 8(*e*) with the corresponding results (out to $G^* = 300$) for $\sigma = 6{\cdot}7$, $\theta'(0) = 0$ obtained by Dring & Gebhart 1968].

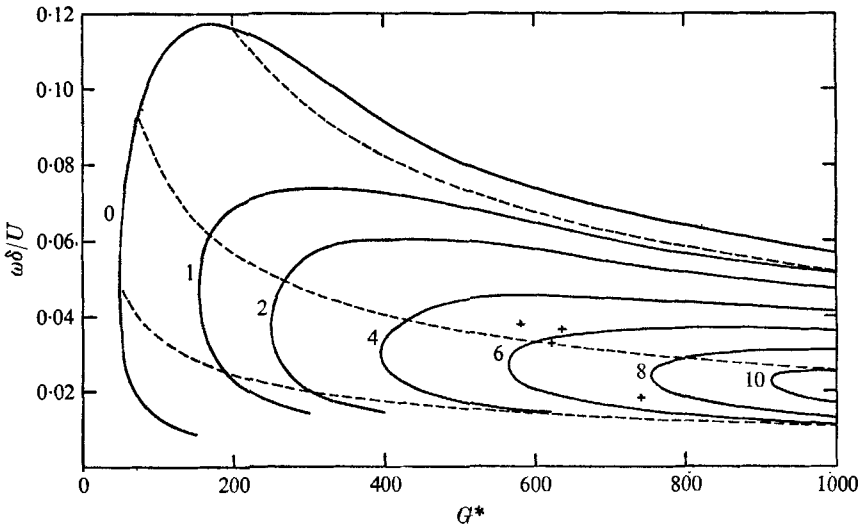

FIGURE 10. Contours of constant $-\frac{1}{4}\int \alpha_i dG^*$ for $\sigma = 6{\cdot}7$, $\theta(0) = 0$. Dashed curves are constant frequency paths. Data: +, Knowles & Gebhart (1969).

Data points, indicating the first appearance of natural disturbances as observed by Eckert & Soehngen (1951), Polymeropoulos (1966) and Knowles & Gebhart (1969), are also indicated in figures 9 and 10. (The first two experiments correspond to $\sigma \approx 0{\cdot}733$, the last to $\sigma \approx 7{\cdot}7$.) Each point being associated with a particular frequency, it is clear these oscillations do not represent turbulence but rather correspond to sinusoidal waves travelling in the vertical direction. The large spread between the data of Eckert & Soehngen (1951) and that of Polymeropoulos (1966) in figure 9 is apparently due to a significant difference in the random disturbance level present in the two experiments, the former being performed in a room, the latter within a pressurized tank. Additional experimental results are indicated below.

Eckert, Hartnett & Irvine (1960), employing a smoke-trace technique in studying the case of an isothermal vertical plate in air, observed a two-dimensional wave pattern in the range $600 \lesssim G^* \lesssim 750$ with the waves propagating in the vertical direction and eventually rolling up into transverse and longitudinal vortices which proceeded to break up abruptly at $G \approx 7{\cdot}3 \times 10^9$ ($G^* \approx 870$).

Szewczyk (1962), in his dye-trace studies in water (at $\sigma \approx 6{\cdot}7$), first observed oscillations at $G \approx 10^9$ ($G^* \approx 600$). Cheesewright (1968), using a thin platinum wire as both a resistance thermometer and a hot-wire anemometer, studied the case of an isothermal vertical plate in air ($\sigma \approx 0{\cdot}733$) and observed the following régimes: first appearance of significant fluctuations at $G \approx 2 \times 10^9$ ($G^* \approx 625$); start of significant changes in the shape of the mean temperature profile (hence, in the local mean heat transfer from the plate) at $G^* \approx 785$; cessation of major changes in the shape of the mean temperature profile at $G^* \approx 885$. Vliet & Liu (1969), employing thermocouples and a hot-film anemometer in studying the case of a uniform-heat-flux plate in water, varied the bulk temperature of the fluid from 45° F to 120 °F (thereby varying σ from 10·5 down to 3·5) and, based upon their data for which $T_w - T_\infty$ was small ($\leqslant 15$ °F), found that the initial transition process (based upon the trend in the local mean heat transfer coefficient) occurred at $G^* \approx 600$, 1000 and 1100 for $\sigma \approx 10$, 6 and 3·5, respectively, with the final stage of transition occurring at $G^* \approx 900$, 1250, 1350.

In terms of G^*, the experimental results are seen to be compatible with the linear stability theory, the interpretation being that ever-present small disturbances in the physical system must first be considerably amplified, as they propagate in the vertical direction towards larger G^*, before becoming discernible to the observer. With respect to $\omega\delta/U$, the theory and the data presented in figures 9 and 10 are seen to be in very good agreement. Furthermore, it is noted that the σ dependence of the transition process observed by Vliet & Liu (1969) is compatible with the theoretical results for $\sigma = 2{\cdot}5$, 6·7 and 25 appearing in figures 8(*d*)–(*f*), the latter implying that, in this range of σ and with G^* fixed,

$$\max\left(-\tfrac{1}{4}\int \alpha_i dG^*\right)$$

increases with σ.

On the basis of the above results for $\sigma = 0{\cdot}733$ and $\sigma = 6{\cdot}7$, it seems reasonable to conclude that, for typical background conditions and any given σ, the natural convection boundary layer arising from a uniform-heat-flux vertical plate can be expected to be noticeably oscillatory at the G^* for which $\max\left(-\tfrac{1}{4}\int \alpha_i dG^*\right) \approx 6$. Seeking an analogous result for the 'onset of turbulence', we note that the first significant changes in the shape of the mean temperature profile observed (at $G^* \approx 785$) by Cheesewright corresponds (in figure 9) to $\max\left(-\tfrac{1}{4}\int \alpha_i dG^*\right) \approx 10$, whereas the corresponding observation (at $G^* \approx 1000$ for $\sigma \approx 6$) by Vliet & Liu corresponds (in figure 10) to $\max\left(-\tfrac{1}{4}\int \alpha_i dG^*\right) \approx 11$. This appears to establish the desired correlation: for typical background conditions and any given σ, the 'onset of turbulence' in the boundary layer arising from a uniform-heat-flux vertical plate can be expected to occur at the G^* for which

$$\max\left(-\tfrac{1}{4}\int \alpha_i dG^*\right) \approx 10.$$

Before concluding, it should be noted that, throughout, it has been assumed that, for a given σ, the cases of an isothermal and a uniform-flux plate can be directly related to each other in terms of G or G^*. (Note for the uniform-flux case, $G^*/G^{\frac{1}{4}} = (125/H(0))^{\frac{1}{4}}$, where H is the non-dimensionalized temperature

defined in §1; for the isothermal plate, $G^*/G^{\frac{1}{4}} = (625|H_1'(0)|/2^{\frac{1}{2}})^{\frac{1}{5}}$ where

$$T - T_\infty \equiv (T_w - T_\infty)H_1(\eta_1), \quad \eta_1 \equiv yG^{\frac{1}{4}}/(2^{\frac{1}{2}}x);$$

in particular, for $\sigma = 0{\cdot}733$ or $6{\cdot}7$, the values of $G^*/G^{\frac{1}{4}}$ for the two cases lie within 3 % of each other). The fact that this led to consistent results, confirms the validity of such an assumption. On the other hand, Vliet & Liu (1969) concluded that the flow arising from a uniform-flux plate is significantly more stable than that of the isothermal case, suggesting that this may be "a result of the basically different fluid dynamics resulting from the two modes of heating". In point of fact, the value which they quoted as the start of transition for the isothermal plate case actually corresponds to $G^* \approx 600$ (for $\sigma = 0{\cdot}733$) and, therefore, to the first appearance of small, two-dimensional oscillations; on the other hand, in determining the start of transition for the uniform-flux case, they employed their own local heat-transfer coefficient data, thereby identifying the start of transition with the first significant change in the mean temperature profile. However, as has been shown above, the régime in which oscillations first appear is not the same as that in which the shape of the mean profile first suffers significant changes, the former corresponding to $\max(-\frac{1}{4}\int \alpha_i dG^*) \approx 6$, the latter to

$$\max(-\tfrac{1}{4}\textstyle\int \alpha_i dG^*) \approx 10.$$

The authors wish to acknowledge the support of the National Science Foundation through research Grants GK 1963 and GK 18529.

REFERENCES

Betchov, R. & Criminale, W. O. 1967 *Stability of Parallel Flows.* Academic.

Cheesewright, R. 1968 Turbulent natural convection from a vertical plane surface. *J. Heat Transfer*, **90**, 1–8.

Colak-Antic, P. 1964 Hitzdrahtmessungen des Laminar-Turbulenten Umschlags bei freier Konvektion. *Jahrbuch* 1964 *der Wissenschaftlichen Gesellschaft fur Luft-und-Raumfahrt E. V.* pp. 172–176.

Drazin, P. G. & Howard, L. N. 1962 The instability to long waves of unbounded parallel inviscid flow. *J. Fluid Mech.* **14**, 257–283.

Dring, R. P. & Gebhart, B. 1968 A theoretical investigation of disturbance amplification in external laminar natural convection. *J. Fluid Mech.* **34**, 541–564.

Dring, R. P. & Gebhart, B. 1969 An experimental investigation of disturbance amplification in external natural convection flow. *J. Fluid Mech.* **36**, 447–464.

Eckert, E. R. G. & Soehngen, E. 1951 Interferometric studies on the stability and transition to turbulence of a free convection boundary layer. *Proceedings of the General Discussion on Heat Transfer, London*, pp. 321–323. (Published by A.S.M.E.).

Eckert, E. R. G., Hartnett, J. P. & Irvine, T. F. 1960 Flow visualization studies of transition to turbulence in free-convection flow. *A.S.M.E. Paper* no. 60-WA-250.

Gebhart, B. 1969 Natural convection flow, instability, and transition. *J. Heat Transfer*, **91**, 293–309.

Gill, A. E. & Davey, A. 1969 Instabilities of a buoyancy-driven system. *J. Fluid Mech.* **35**, 775–798.

Hieber, C. A. & Gebhart, B. 1971 Stability of vertical natural convection boundary layers: expansions at large Prandtl number. To appear in *J. Fluid Mech.*

KAPLAN, R. E. 1964 The stability of laminar incompressible boundary layers in the presence of compliant boundaries. *Mass. Inst. Tech., Aeroelastic & Structures Research Lab.* TR 116–1.

KNOWLES, C. P. & GEBHART, B. 1968 The stability of the laminar natural convection boundary layer. *J. Fluid Mech.* **34**, 657–686.

KNOWLES, C. P. & GEBHART, B. 1969 An experimental investigation of the stability of laminar natural convection boundary layers. *Progress in Heat and Mass Transfer*, vol. 2. Pergamon.

KURTZ, E. F. & CRANDALL, S. H. 1962 Computer-aided analysis of hydrodynamic stability. *J. Math. Phys.* **41**, 264–297.

MACK, L. M. 1965 Computation of the stability of the laminar compressible boundary layer. *Methods in Computational Physics*, vol. 4. Academic.

MORAWETZ, C. S. 1952 The eigenvalues of some stability problems involving viscosity. *J. Rat. Mech. Anal.* **1**, 579–603.

NACHTSHEIM, P. R. 1963 Stability of free-convection boundary layer flows. *NASA TN* D-2089.

OSTRACH, S. 1964 Laminar flows with body forces. In *Theory of Laminar Flows* (ed. F. K. Moore). Princeton University Press.

OSTRACH, S. MASLEN, S. H. 1961 Stability of laminar viscous flows with a body force. *Int. Heat Transfer Conf., University of Colorado*, 1017–1023. (Published by A.S.M.E.).

PLAPP, J. E. 1957 Laminar boundary layer stability in free convection. Ph.D. Thesis, Calif. Instit. Tech.

POLYMEROPOULOS, C. E. 1966 A study of the stability of free convection flow over a uniform flux plate in nitrogen. Ph.D. Thesis, Cornell University.

POLYMEROPOULOS, C. E. & GEBHART, B. 1967 Incipient instability in free convection laminar boundary layers. *J. Fluid Mech.* **30**, 225–239.

SMITH, A. M. O. 1957 Transition pressure gradient and stability theory. *Proc. 9th Int. Congress of Appl. Mech., Brussels*, **4**, 234–244.

SPARROW, E. M. & GREGG, J. L. 1956 Laminar free convection from a vertical plate with uniform surface heat flux. *Trans. A.S.M.E.* **78**, 435–440.

SPARROW, E. M., TSOU, F. K. & KURTZ, E. F. 1965 Stability of laminar free convection flow on a vertical plate. *Phys. Fluids*, **8**, 1559–1561.

SZEWCZYK, A. A. 1962 Stability and transition of the free-convection layer along a vertical flat plate. *Int. J. Heat Mass Transfer*, **5**, 903–914.

VLIET, G. C. & LIU, C. K. 1969 An experimental study of turbulent natural convection boundary layers. *J. Heat Transfer*, **91**, 517–531.